Techno-economic optimization of an offshore hybrid power system: Argentine Basin case study

Sarah May Palmer, Trent Dillon, and Brian Polagye

Abstract—**Temporally continuous and spatially distributed measurements of Essential Ocean Variables are required to improve our understanding of the Earth's oceans. These measurements can be provided with combinations of moored platforms and uncrewed underwater vehicles, but with substantially higher power costs than conventional ocean observation. While these power needs could be provided by a single source of generation and battery storage, a hybrid power system can potentially smooth seasonal variations and reduce required generation and storage capacities. To this end, we develop an optimization model to identify minimum-capacity hybrid power systems for a given location and load profile. The model considers generation by wave energy converters, wind turbines, solar photovoltaics, diesel generators, and current turbines with a battery for energy storage. The model uses the load profile and resource time series in a time-domain simulation of the battery state of charge to calculate persistence. The optimization model searches the design space for the system with the minimum objective function value that can satisfy persistence requirements. In this paper, we focus on a case study of a hybrid power system serving an ocean observation buoy with a resident UUV located at Argentine Basin. As expected, identified hybrid systems have smaller aggregate capacity than the single generator cases, but the search for minimum-capacity systems within a five-dimensional design space demonstrates the complexity of hybrid optimization. Results show that hybridization is beneficial, but that optimization to more nuanced metrics, like system cost, will be challenging.**

Index Terms—**hybrid power, ocean observation, techno-economic optimization, blue economy**

I. Introduction

OCEAN observation platforms paired with resident uncrewed underwater vehicles (UUVs) are potentially well-suited to long-term, spatially-distributed oceanographic data collection. Such observations of Essential Ocean Variables are a current focus for Global Ocean Observing Systems [1]. However, the resolution and scope of data collection by these systems is limited by power availability and energy storage [2]. In-situ power for ocean observation systems can be generated from a variety of sources including, diesel generators [3], solar panels [4] [5], wave energy converters (WECs) [6] [7] [8] [9] [10], wind turbines [11], and current turbines [12]. Each generator option has disadvantages, particularly in offshore environments: diesel generators have finite endurance and require expensive refueling operations, photovoltaic panel performance can be hindered by resource availability [13] and soiling [14], wind turbines can reduce platform stability [14], and WECs and current turbines are developing technologies with unproven reliability.

Hybrid power systems, combining multiple generation sources, provide redundancy [11] and increase total power generation for a given platform footprint [15], [16]. Furthermore, a hybrid power system tailored to a location's specific resource availability can potentially serve a load with less total generation and storage capacity than would be required for a single-resource system. The optimization of hybrid power system design for oceanographic sites and load profiles is functionally similar to the analysis that HOMER conducts for remote, land-based hybrid power systems [17]. However, HOMER does not include WECs and is not designed for the specific economics of floating offshore power systems (e.g., vessel based maintenance/refueling operations, mooring costs).

There are limited examples of techno-economic analyses for floating power system design [18], [19], [20]. Previously, Dillon et al. [19] defined a cost-optimal power system for an ocean observation platform using a wave energy converter and battery. The optimization was performed for a constant, 200 W load case at five deployment locations. Subsequent analysis [18] expanded to consider photovoltaic panels, wind turbine, or diesel generators at a subset of these locations. The single-resource optimization shows that system capacity requirements can be dramatically higher for locations with significant seasonal resource asymmetry. This suggests that hybrid power systems could substantially reduce required generation and storage.

Here, we present a hybrid power system optimization based on the previously-developed single-resource models in [18]. The hybrid systems incorporate a mix of solar, wind, wave, current, and/or diesel generators, as well as battery storage. We consider the system's application to a load case corresponding to power-intensive ocean observation and periodic UUV recharge. As a preliminary step to economic optimization, we employ power system aggregate capacity as the optimization

© 2023 European Wave and Tidal Energy Conference. This paper has been subjected to single-blind peer review.

This work is funded by Naval Facilities Engineering and Systems Command under contract N0002421D6400/N0002421F8712

S. M. Palmer is with Department of Mechanical Engineering, University of Washington Seattle, WA, U.S.A (e-mail: smp52@uw.edu).

T. Dillon is with Department of Mechanical Engineering, University of Washington Seattle, WA, U.S.A (e-mail: tmaxd@uw.edu).

B. Polagye is with Department of Mechanical Engineering, University of Washington Seattle, WA, U.S.A (e-mail: bpolagye@uw.edu).

Digital Object Identifier:
https://doi.org/10.36688/ewtec-2023-399

target for the hybrid power system, using this to gain insight into hybrid platform design and assess hybridization benefits. Aggregate capacity scales with system size, which is also an important consideration for the feasibility of offshore operations.

The remainder of this paper is organized as follows. Section II describes the mission definition, location-specific resources, and the energy generation, aggregate capacity, and optimization models. Section III presents the optimal system definitions for single-resource and hybrid systems, as well as visualizations of the design space near the minimum aggregate capacity power system. Section IV discusses the behaviors and limitations of different optimization algorithms, as well as next steps in this analysis.

II. Methods

The following subsections outline the components and implementation of the hybrid power system optimization model. This is an extension of the single-resource optimization models developed by Dillon et al. [18], [19]. The optimization objective is to find the smallest aggregate capacity system ($\min(J_{\text{total}})$), that can satisfy a "persistence" requirement ($a_{\text{sim}} \geq 0.99$). Persistence refers to the fraction of the intended load that is met by the power system. Because of the stand-alone nature of the system, persistence must be assessed by time domain simulation of resource availability, storage, and load. Figure 1 provides an overview of the modeling framework, including free parameters, model constants, input time series, and approaches to optimizing the free parameters. For a given six-dimensional design space (one for each of the five resources and one for battery storage), each iteration of the optimization model identifies the persistence and aggregate capacity across a range of power system capacities. The optimization model is formatted such that the result of multiple iterations is the minimum aggregate capacity power system that satisfies the persistence constraint. The challenges to this optimization are the non-smooth nature of the design space and the number of unique power systems that must be evaluated in the time domain.

A. Ocean Observing Operations Concept

The power system is optimized to meet the specified load requirements given the time series of resource availability at the deployment location. While the model can be adjusted for various platform designs, maintenance schedules, and load profiles, the mission design used in this analysis is as follows. The load corresponds to an oceanographic instrumentation package with periodic uncrewed underwater vehicle (UUV) recharging (Figure 2). Power is provided by a notional buoy. The mission life is six years with a comprehensive maintenance (entire power system replaced with a spare and refurbished on shore) every two years. This operations concept constrains the diesel generation case, since refueling and oil changes are restricted to comprehensive maintenance intervals. During maintenance, if the battery's capacity has faded by more than 20% [21] as a result of degradation, it is replaced. Time series for solar irradiance, wind speed, and sea state (significant wave height, H_s, and peak period, T_p) are obtained from the National Science Foundation's Ocean Observatories Initiative (OOI) buoy at Argentine Basin (42.99 S, 42.5 W) at roughly hourly resolution [23]. This location does not have significant currents, but is adjacent to regions with moderate ocean currents. For this analysis, a composite location ("Modified Argentine Basin") was formulated with solar/wind/wave resources consistent with Argentine Basin, and current resources from the Hybrid Coordinate Model (HYCOM, [24] at 41.25 S, 52.03 W). The current data was in 3 hour intervals at water depths 0 m to 300 m. The monthly average power density of all four resources are summarized in Figure 3.

The start and end times in the solar/wind/wave data from OOI were chosen to obtain continuous datasets. Measurement gaps (1-3 hr) and outliers were replaced with interpolated data [18], [19]. The datasets have two requirements to be valid inputs to the time domain simulation: the time series data for each resource must be as long as the mission life, and the seasonal and diurnal patterns of the resources must be properly aligned. To meet these requirements we created a data cleaning function that uses shorter and misaligned input data as inputs. The cleaning function interpolated the raw data to an hourly basis (the current velocity was assumed to be constant between each 3 hour interval). Datasets shorter than a year were extended by duplicating data from a month equidistant from January for the missing months. Then all the datasets were duplicated to cover the six year mission life. Lastly, the datasets were aligned so they all start on the same day and same hour by duplicating data from a year in the future for any missing time steps. Extending and aligning the data in this manner assumes that inter-annual variations are generally subordinate to seasonal variations. Future analysis will consider longer duration data series to capture inter-annual variation.

B. Energy Modeling

The central quantity of the energy model is the battery state of charge, which evolves based on the current state of charge, battery self discharge, $\Gamma(S(t))$, power produced by all resources, $P_{\text{total}}(t)$, power draw, $L(t)$, and excess energy discarded, $D(t)$. This is mathematically described as

$$S(t+1) = S(t) - \Gamma(S(t)) + \Delta t(P_{\text{total}}(t) - L(t)) - D(t). \quad (1)$$

$P_{\text{total}}(t)$ is the sum of power produced from all resources:

$$P_{\text{total}}(t) = P_{\text{solar}}(t) + P_{\text{wind}}(t) + P_{\text{wave}}(t) + P_{\text{current}}(t) + P_{\text{diesel}}(t) \quad (2)$$

where the power from each generator is assumed to be constant over an hour-long interval. The calculation of power from the PV panels, wind turbine, and WEC follow the same equations as the single resource models [19], [18], overviewed as follows.

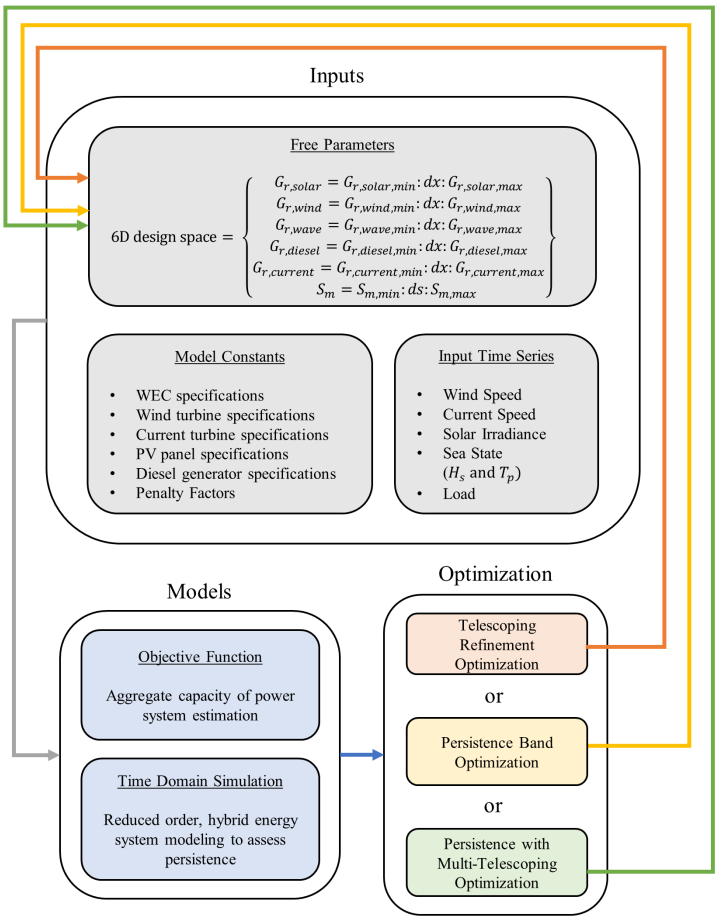

Fig. 1. Optimization procedure for the hybrid model. The free parameters (generator rated power and battery capacity), model constants, and input time series are used in the time domain simulation to determine persistence. During each iteration, the time domain simulation and aggregate capacity estimation are evaluated for every point in a design space with up to six dimensions. The results are used to update the design space for the next iteration.

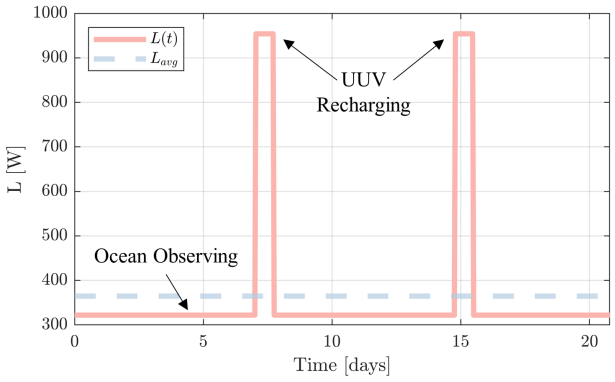

Fig. 2. Load profile ($L(t)$) for power-intensive ocean observation platform with periodic UUV recharging. The ocean observing load is a constant 322 W, modeled after the Adaptable Monitoring Package [22]. The UUV recharging, patterned after wireless recharge of a Remus 600 UUV, requires an additional 632 W for 17 hours and occurs every 7 days. Time series is shown for 20 days, but the pattern repeats for the entire 6 year mission.

For the photovoltaic panels, we assume a panel efficiency of 18% and an automated cleaning mechanism to prevent soiling, with power (P_{solar}) calculated as,

$$P_{\text{solar}} = \begin{cases} \eta_{deg_t} G_{r,\text{solar}}\left(\frac{i(t)}{i_r}\right) & i(t) \leq i_r \\ \eta_{deg_t} G_{r,\text{solar}} & i(t) > i_r \end{cases} \tag{3}$$

where $i(t)$ is the irradiance at time t, $i_r = 1\text{kW/m}^2$ is the rated irradiance, and $\eta_{deg,t}$ is the efficiency loss due to panel aging (0.5% per year [25]).

Wind turbine power (P_{wind}) is calculated as a function of wind speed adjusted to turbine hub height,

$$P_{\text{wind}} = \begin{cases} 0 & u_w(t) < u_{w,ci} \\ G_{r,\text{wind}}\left(\frac{u_w(t)^3}{u_{w,ra}^3}\right) & u_{w,ci} < u_w(t) \leq u_{w,ra} \\ G_{r,\text{wind}} & u_{w,ra} < u_w(t) \leq u_{w,co} \\ 0 & u_w(t) > u_{w,co} \end{cases} \tag{4}$$

where $u_w(t)$ is the wind velocity at the turbine hub height as a function of time, t, $u_{w,ci}$ is the wind turbine cut-in speed (3 m/s), $u_{w,ra}$ is the rated speed (11 m/s), and $u_{w,co}$ is the cut-out speed (30 m/s). These values are consistent with American Wind Energy Association (AWEA) standards [26]. The turbine rotor clearance above the water surface is 4 m, with a rotor radius given by,

$$R_{\text{wind}} = \sqrt{\frac{2G_{r,\text{wind}}}{\eta_w \pi \rho_a u_{w,ra}^3}} \tag{5}$$

where $\eta_c = 0.35$ is the assumed wind to wire efficiency, and ρ_a is air density (1.225 kg/m^3).

To find WEC power output, WEC capture width ratio (CWR) is treated as a function of WEC size

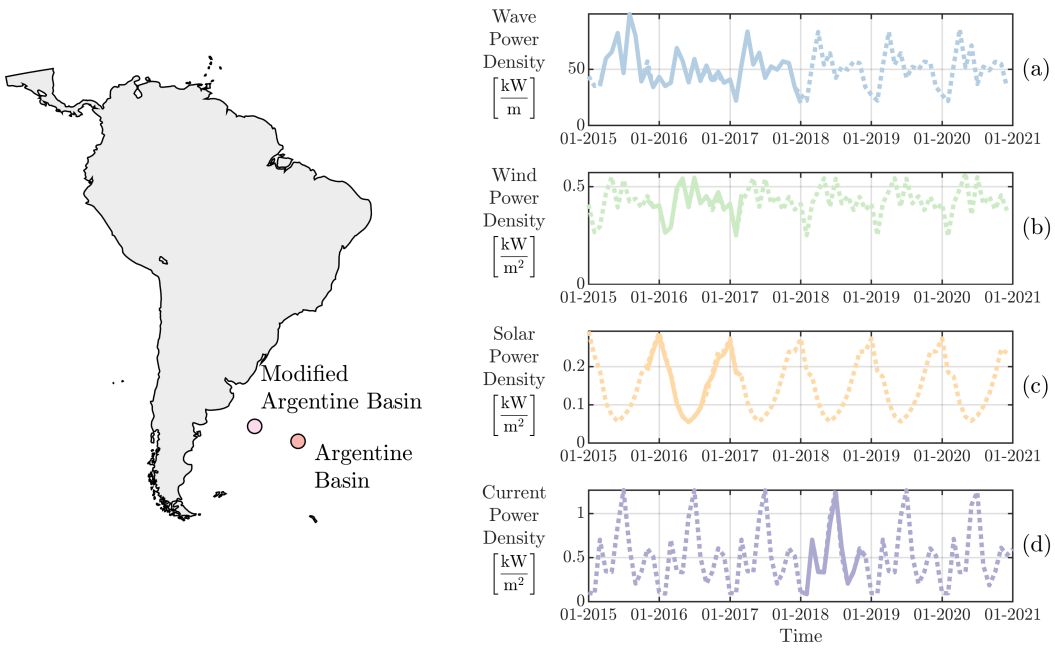

Fig. 3. The optimal hybrid system depends on the location-specific resource time series. The wave (a), wind (b), and solar (c) resource time series are datasets from Argentine Basin. The current (d) dataset is HYCOM data from Modified Argentine Basin. The current power density is shown at a depth of 4 m, which is the approximate center plane depth of the turbine. The solid lines are the raw data and the dotted lines are the cleaned and aligned datasets. Note that the y-axis scale is different for each resource, and the definition of wave power density is not directly comparable to the other resources.

and sea state and calculated via linear interpolation of WEC-Sim results for scaled Reference Model 3. Power (P_{wave}) is calculated as,

$$P_{\text{wave}} = \eta_{wec} CWR * B \left[\frac{\rho_w g^2 H_s(t)^2 T_p(t)}{64\pi} \right] - hG_{r,\text{wave}} \tag{6}$$

where $\eta_{wec} = 0.6$ is the electrical conversion efficiency, B is WEC width, $\rho_w = 1025\ \text{kg/m}^3$ is sea water density, $H_s(t)$ is the wave height as a function of time, $T_p(t)$ is the peak wave period as a function of time, $g = 9.81\ \text{m/s}^2$ is the gravitational constant, and h is the percentage of the WEC's rated capacity used to power "house loads" (assumed to be 10% of the WEC's rated power). The maximum value of P_{wave} is set to $G_{r,\text{wave}}$.

Power from the current turbine (P_{current}) is a function of current speed at center plane depth that mirrors the wind model where $u_c(t)$ is the current velocity at the turbine center plane depth as a function of time, t, $u_{c,ci}$ is the current turbine cut-in speed (0.5 m/s), $u_{c,ra}$ is the rated speed (2 m/s), and $u_{c,co}$ is the cut-out speed (3 m/s). These values are consistent with reference models [27]. The turbine rotor is assumed to have 1.5 m clearance with the water surface (0.5 m clearance with a notional 1 m platform draft). For a cross-flow turbine with an aspect ratio of unity, the rotor frontal area is square, with a characteristic dimension

$$R_{\text{current}} = \sqrt{\frac{2G_{r,\text{current}}}{\eta_c \rho_w u_{c,ra}^3}} \tag{7}$$

where $\eta_c = 0.28$ is the current turbine current to wire efficiency (based on engineering judgement of $C_{p,max} = 0.4$ and $\eta_o = 0.7$).

The diesel generator runs for one hour ($P_{\text{diesel}}(t) = G_{r,\text{diesel}}$) if the battery state of charge is insufficient to satisfy the load for the next hour. The number of hours the diesel generator runs ($T_{\text{run,int}}$) and the volume of fuel consumed between maintenance intervals is tracked. If the runtime exceeds 250 hours (oil change required) or the fuel volume consumed exceeds 800 L, then this is considered unachievable without additional vessel intervention [18].

The battery is a lithium iron-phosphate (LFP) chemistry. The storage capacity decreases over time due to calendar aging and cyclic loading. Therefore the capacity of both batteries (one for the active buoy and one for the spare) must be tracked to calculate degradation using Xu et al.'s model [21] for battery degradation under irregular cycling. The battery that begins the mission on shore does not have a cyclic charge profile for the first two years, so the capacity fading is calculated with only calendar degradation over that time.

The ability of the power system to satisfy the load requirements of the instrumentation and UUV charging is assessed by "persistence" which is defined as,

$$a_{\text{sim}} = \frac{\Sigma_{t=1}^{N} L(t) = L_c(t)}{N} \tag{8}$$

where L is the time series of load supplied to the instrumentation and vehicle charging system, L_c is the desired load time series, and N is the number of hours in the mission life. If $a_{\text{sim}} \geq 0.99$ then the power system is considered sufficient for the load profile and a viable case.

C. Objective Function: Aggregate Capacity

The optimization target for this preliminary analysis is minimum power system aggregate capacity. In this

approach, we assume that a larger system is less desirable, and therefore calculate a "penalty" associated with the capacity of each generator and battery for each point in the design space. The sum of these penalties, including spares and replacements, is the aggregate capacity. The point with the lowest aggregate capacity that satisfies the persistence requirements is the "optimal" system. The penalty associated with one buoy's power system, J_{system}, is given as

$$J_{\text{system}} = J_{pv} + J_{wt} + J_d + J_{lfp} + J_{wec} + J_{ct} \quad (9)$$

where J_{pv} is the photovoltaic (PV) module penalty, J_{wt} is the wind turbine penalty, J_d is the diesel generator penalty, J_{lfp} is the lithium-iron-phosphate (LFP) battery penalty, J_{wec} is WEC penalty, and J_{ct} is the current turbine penalty. The operations concept requires two platforms, so the aggregate capacity is twice the penalty of a single power system plus the penalty of any additional batteries needed to replace a depleted battery prior to end of the deployment. Therefore, the aggregate capacity is defined as

$$J_{\text{total}} = 2 \times J_{\text{system}} + N_{lfp} \times J_{lfp}. \quad (10)$$

where N_{lfp} is the number of additional battery modules required during the mission.

Component penalties are defined as the rated power of the generator, or maximum capacity of the battery weighted by an equivalence factor. The component penalties used in the model are shown in Table I. The factor applied to the battery is based on the mass of LFP batteries and an aluminum enclosure. The factor applied to all the generators is based on the unit mass of a wind turbine. The choice of a constant factor on all generators simplifies the optimization space, while maintaining a physical relationship between the generator and battery penalties. Additionally, defining the optimization target this way allows for analysis of resource compatibility, absent other differences between the generation sources, and the theoretical limits to benefits of hybridization.

The $80\ \text{kg/kW}$ constant for wind turbine mass includes the unit mass (mass/rated power) of the turbine (AIR 403 turbine [28], [29]) and the unit mass of the tower (Schedule 40 Aluminum pipe [28]). The AIR 403 design uses a guyed tower which is not feasible for this application. Therefore 4x the pipe mass is used to account for the truss structure of the tower, albeit with high uncertainty.

The specific energy of the lithium-iron-phosphate (LFP) battery is approximately $105\ \text{Wh/kg}$ [30]. The battery enclosure mass is calculated using a non-negative linear regression of volume vs. rated storage capacity for 13 LFP batteries. The surface area of a cube that encloses the battery volume and an assumption of 1.27 cm (0.5 inch) aluminum plate ($35\ \text{kg/m}^2$) [31] yields the associated enclosure mass. A limitation is that the library of LFP batteries are all < 1 kWh capacity, so the extrapolation to larger capacities is uncertain.

If the optimization algorithm finds multiple systems that satisfy the persistence requirement and have the same aggregate capacity then the algorithm checks each of those systems to find those with the minimum total generation capacity (i.e., sum of individual generator capacities). If there are multiple systems that have the same minimum aggregate capacity and minimum total generation capacity, then the model determines that there are multiple, equivalent representations of an optimal system.

D. Optimization Methods

For optimization, the design space consists of a six-dimensional matrix defined by the rated capacities for each generation source (G_r) and initial battery storage capacity (S_m). The maximum rated capacity for any generation source is set at 8 kW, the minimum capacity is 0 kW (i.e., the model can opt not to include a generation source), and the battery capacity is between 1 and 500 kWh. The battery minimum is set to 1 kWh because energy storage is always required to smooth resource intermittencies for the renewable power sources. The maximum grid size is increased if the minimum aggregate capacity system definition is at a corner of the defined design space (minimum/maximum G_r or S_m).

The optimization model must search the design space for the system with the lowest aggregate capacity that meets the load persistence requirement. The simplest option is to calculate aggregate capacity and persistence for all possible combinations of storage capacity and generator sizes, then identify the minimum. While this approach was employed for single-resource optimization in [18], [19], if the design space grid is well-resolved (e.g., 500 points in each dimension), the hybrid model would require 1.5×10^{16} evaluations of the time domain simulation – which is computationally prohibitive. Therefore, multiple alternative optimization algorithms were developed and tested. The three algorithms were implemented in MATLAB and executed on one node (40 CPUs and 363 GB of memory) of UW's high-performance computing cluster (Klone-Hyak).

The first is referred to as "telescoping refinement" (Figure 4 (a)). Telescoping refinement increases the resolution of the design space around the minimum aggregate capacity point from the previous iteration. The first iteration discretizes the design space into nine points for each dimension, evaluates the time domain simulation on the coarse grid, and identifies the minimum aggregate capacity point. Then the grid boundaries are adjusted to one point away from the minimum in each dimension and this "zoomed-in" space is discretized with nine points in each dimension. This process is repeated until the minimum-aggregate capacity configuration between iterations has converged to a tolerance of 1% for aggregate capacity, as well as storage capacity and generator capacities. If the telescoping refinement algorithm does not converge, then the optimization ends after 5 iterations (final generation capacity resolution of 0.002 kW).

The second optimization algorithm is referred to as "persistence band" (Figure 4 (b)). Persistence band optimization refines the design space in the region

TABLE I
COMPONENT PENALTY CALCULATIONS

Component Penalty	Reference	Equation
Generator	AIR 403 turbine [28], [29]	$J_g = 80\ [\mathrm{kg/kW}] \times G_r$
LFP Battery Pack	LFP specific energy [30]	$J_{lfp,p} = S_m/0.105\ [\mathrm{kWh/kg}]$
Battery Enclosure	13 - LFP battery volumes	$J_{lfp,e} = 6 \times (0.002\ [\mathrm{m^3}] + 0.0012\ [\mathrm{m^3/kW}] \times S_m)^{2/3} \times 35.24\ [\mathrm{kg/m^2}]$
Battery System	$\sim$	$J_{lfp} = J_{lfp,p} + J_{lfp,e}$

surrounding the 6D-surface of 99% persistence. This optimization method relies on the knowledge that the minimum-aggregate capacity configuration will lie on the 6D-surface of 99% persistence (since further aggregate capacity reduction would fail to satisfy the persistence requirement). The first iteration is identical to telescoping refinement. Once this coarse design space is populated, the points in the space with persistence values near the target value of 99% (e.g., 97.5% to 99.5%) define the region of interest. During each subsequent iteration, the grid discretization is doubled, but only points with persistence within in the region of interest are retained. This process is repeated for 5 iterations (final generation capacity resolution of 0.06 kW).

As discussed in Section IV, neither algorithm achieves entirely satisfactory results. The telescoping algorithm has limited accuracy when the regions of minimum aggregate capacity are non-continuous and/or non-monotonic, and the persistence algorithm has grid discretization and runtime limitations. Therefore, these were combined into a third algorithm referred to as "persistence with multi-telescoping". For the first three iterations, the design space is refined using the persistence algorithm. For the fourth and fifth iterations, where further refinement with the persistence algorithm becomes computationally intensive, all points that have a aggregate capacity similar to the minimum aggregate capacity define the points of interest. At every point of interest, additional points in each dimension are added to the design space in the region defined by one point away in each dimension from the point of interest (i.e., a telescoping grid is applied to each point of interest). This algorithm completes after 5 iterations (final generation capacity resolution of 0.065 kW). The upper and lower bounds of the points that are in the region of interest for the persistence iterations, the upper and lower bounds of the points of interest for the telescoping iterations, and the number of points applied in each telescoping grid can be adjusted. The choice of these parameters affects the final grid resolution, and the portions of the design space that are discretized to the final resolution. Therefore, these input parameters affect the identification of "optimal" hybrid systems.

III. RESULTS

Since the mission design and load case are significantly different than those in Dillon et al. [18], the hybrid results cannot be directly compared to prior single-resource results. Therefore, we begin by presenting contextual results for single-resource design

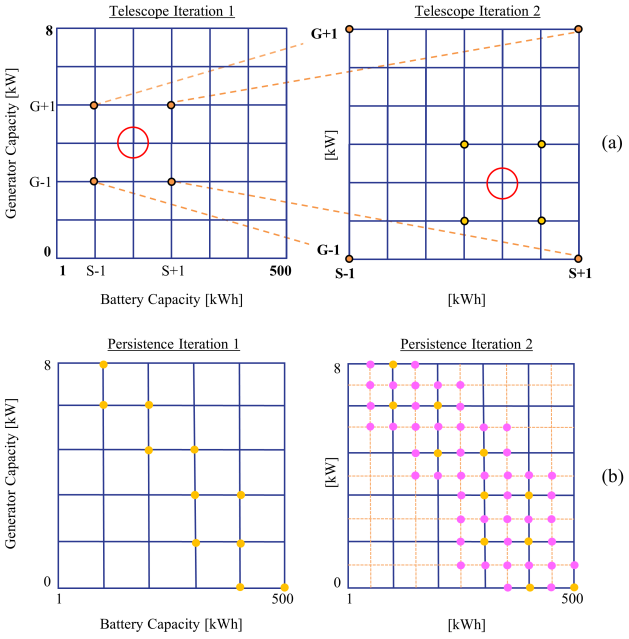

Fig. 4. The telescoping refinement optimization algorithm (a) finds the minimum aggregate capacity point in the first grid, then redefines the grid boundaries to be one point away from that minimum. The persistence band optimization algorithm (b) identifies the points in the region of interest (yellow points), and finds the points near that band in the next iteration's grid (pink points). While these figures show the optimization in two dimensions, the actual optimization occurs in up to six dimensions.

spaces consisting of one generation source and storage. Unlike the hybrid optimization algorithms, the single-resource cases involve calculating aggregate capacity at every point on a 500x500 grid (generation x storage) and identifying the system with the lowest aggregate capacity that satisfies the persistence threshold. Table II shows the minimum aggregate capacity system definition, persistence, and aggregate capacity for each single-resource space. Depending on the resource, optimal G_r varies from 2.3 to 15 kW and S_m varies from 18 to 217 kWh. This variation reflects differences in resource power density and consistency at the location. The smallest single-resource system uses wind generation, $J_{\text{total}} = 759$. This system is the benchmark for hybrid optimization, since that algorithm can choose a single-resource system if it is optimal. We note that no solution is found for the diesel generator case because the diesel generator is poorly matched to this mission due to the prescribed fuel volume consumption and runtime limits.

To decrease the computational time required for this

TABLE II
SINGLE-RESOURCE OPTIMIZATION PARAMETERS AND RESULTS

Optimization Parameters				
Algorithm	Comprehensive (500 × 500 grid)			
Grid Discretization	0.016 kW, 0.998 kWh			
Results				
Case	G_r [kW]	S_m [kWh]	a_{sim} [%]	J_{total}
Solar-only	6.6	22	99	1529
Wind-only	2.3	18	99	759
Wave-only	3.3	26	99	1085
Current-only	15.0[a]	217	99	6769
Diesel-only	N/A	N/A	N/A	N/A

[a] The minimum current capacity that satisfied the persistence threshold is at the edge of the original design space (8 kW maximum capacity), so the design space was expanded to 15 kW. The capacity for the actual case is slightly < 15 kW.

TABLE III
HYBRID OPTIMIZATION PARAMETERS AND RESULTS

Optimization Parameters		
Algorithm	Persistence with Multi-Telescoping	
Grid Discretization	0.07 kW, 4.04 kWh	
Persistence Band	$0.975 < a_{sim} < 0.995$	
Telescoping Points	$0.97 \times J_{\text{total},min} < J_{\text{total}} < 1.03 \times J_{\text{total},min}$	
Results		
	No Current	No Diesel
$G_{r,\text{diesel}}$	0.08 kW	N/A
$G_{r,\text{current}}$	N/A	0.08 - 0.24 kW
$G_{r,\text{solar}}$	0.75 kW	0.75 kW
$G_{r,\text{wind}}$	1.24 kW	0.96 - 1.21 kW
$G_{r,\text{wave}}$	0.68 kW	0.59 - 0.84 kW
S_m	9.02 kWh	9.02 kWh
a_{sim}	99.2%	99 - 99.02%
J_{total}	643	630

Fig. 5. Time series of battery state of charge (a), generated power (b), power discarded (c), and supplied load (d) for the optimal **single - resource system**. Only the first year of the mission life is shown. The power discarded (c) shows the generation by the system in excess of load requirements and storage capacity. The load time series (d) generally follows the commanded load (see Figure 2), except for cases when the battery state of charge is too low and the supplied load drops to zero.

preliminary analysis, the largest optimization space analyzed is five-dimensional (four generation sources and storage). This was completed by forcing the size of the generation source excluded from the analysis to always be zero. Two hybrid cases are considered. The first is a solar-wind-wave-diesel-battery system (no current turbine). This design space contains the three co-located renewable sources at Argentine Basin. The second case is a solar-wind-wave-current-battery system (no diesel generator), representing a system powered solely by renewable sources. This design space uses the current data from the "Modified Argentine Basin" location. Optimal capacity combinations are identified within these design spaces using "persistence with multi-telescoping" algorithm. Optimization parameters and results are presented in Table III. Both design spaces contain systems with a smaller aggregate capacity than the smallest single-resource system. The range of generator sizes shown for the case without diesel is a consequence of multiple optimal aggregate capacity systems found for that case. For both systems, the battery size is smaller than for the single-resource cases and the individual generators are also lower capacity. This is a consequence of the mix of generation capacity able to access differing resource availability at this location.

Having identified capacity-optimal single-resource and hybrid generation scenarios, we now consider the time-domain behavior of these systems, which underpins the optimization process. Figure 5 shows the system behavior for the single-resource system with the smallest aggregate capacity (wind-battery system). The average power discarded for this case is 0.7 kW. In contrast, the optimal hybrid system excluding the current turbine has an average power discarded of 0.6 kW, and the optimal hybrid system excluding the diesel generator shown in Figure 7 has an average power discarded of 0.5 kW. Figure 6 shows the system behavior for the hybrid optimal system excluding the current turbine. While the diesel generator was ineffective for the single-resource optimization, in this hybrid case, a small (0.08 kW) diesel generator is optimal. The diesel generator only turns on during minimums in the renewable resources when the battery state of charge is too low to meet the commanded load. Significant generation, in excess of load requirements and storage capacity, is discarded (Figure 6f). The power system size must be sufficient to meet the UUV recharge load during limited resource availability, which results in excess power generation when the UUV is not charging and/or when the resource availability is more than sufficient.

When diesel generation is excluded from the hybrid optimization, there are 16 equivalent, optimal power systems with the same objective function value and same total generation capacity. The time series for one of these systems is shown in Figure 7. The seasonal trends in solar irradiance and ocean current speed are complementary at this location so when the power

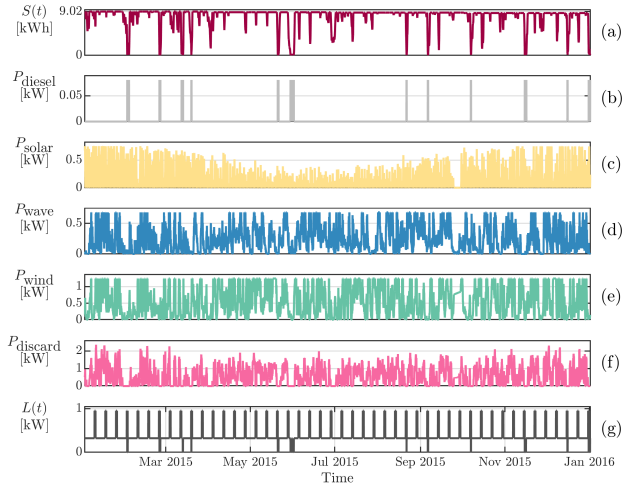

Fig. 6. Time series of battery state of charge (a), generated power (b-e), power discarded (f), and supplied load (g) for the optimal **hybrid system with no current turbine**. Only the first year of the mission life is shown. The power generated by the PV panels, WEC, and wind turbine are functions of resource availability, but are limited to the generator rated power. The power discarded (f) shows the generation by the system in excess of load requirements and storage capacity. The load time series (g) generally follows the commanded load (see Figure 2), except for cases when the battery state of charge is too low and the supplied load drops to zero.

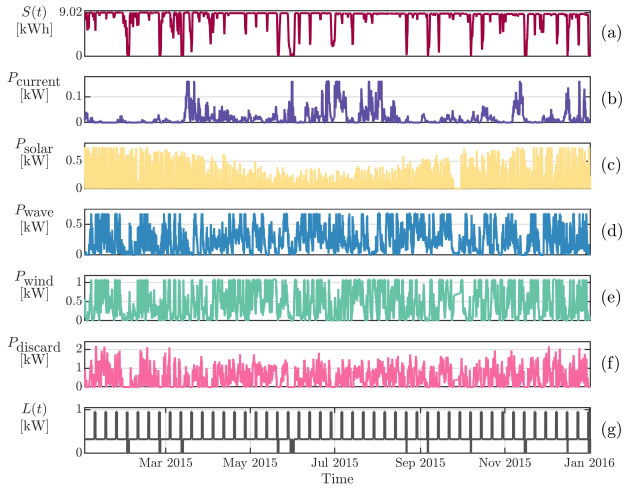

Fig. 7. Time series of battery state of charge (a), generated power (b-e), power discarded (f), and supplied load (g) for one of the 16 optimal **hybrid systems with no diesel generator**. Time series representation of system performance as for Figure 6

output of the solar panel decreases in the summer, the power output of the current turbine increases. This allows for smaller total generation capacity and a smaller aggregate capacity (J_{total}) than when current turbine is excluded in favor of diesel generation. The capacities of the generators vary between each of the 16 optimal power systems defined for the hybrid system excluding the diesel generator. The system definition for each of the 16 optimal combinations are shown in Figure 8. As previously discussed, when the optimization algorithm finds multiple points with the minimum aggregate capacity, it checks each power system's total

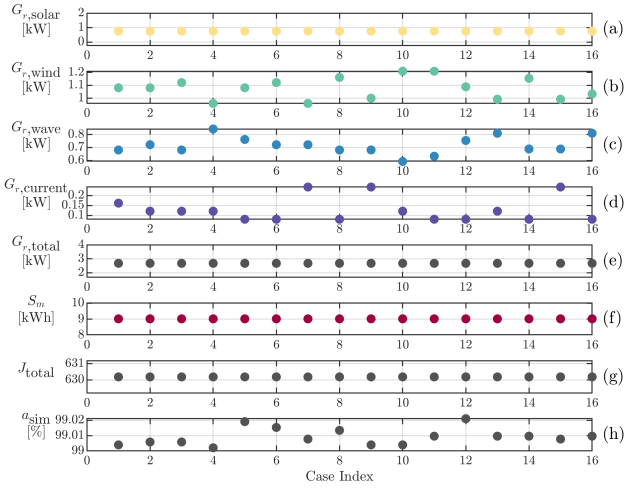

Fig. 8. The 16 optimal points in the **hybrid design space excluding the diesel generator**. The free parameters of the design space are the four generator capacities (a-d), and battery max capacity (f). Total generation capacity for each system is shown in (e). Additionally, the corresponding aggregate capacity (g) and persistence (h) are shown for each point. The x-axis value represents a case index, and the values of the free parameters, total generation and aggregate capacity are the corresponding values for that case. Note that the axes limits are different for each generator.

generation capacity and only keeps points with the minimum total generation capacity (i.e., all 16 optimal points have the same total generation capacity and, by definition, all the optimal systems also have the same battery maximum capacity). However, the mix of hybrid generation varies between each optimal system, and the persistence value deviates slightly from the threshold value (99%) due to design space resolution. All systems employ the same solar capacity but the mix of wind turbine, current turbine and WEC rated capacity vary. The range of rated capacities for the current turbine are much lower than those for the WEC and wind turbine, which is a result of the inconsistency of the current resource at this location.

Representing the entire design space for the single-resource optimization can be achieved with a surface plot of aggregate capacity at each point in the design space. However, for hybrid design spaces, visualization is less straightforward. Each point in the design space has a unique case index that corresponds to a unique set of values for each free parameter, aggregate capacity, and persistence. Plotting the values of free parameters and aggregate capacity at each index can be thought of as an "unwrapped" 5D optimization space. Visualizations of the points in the hybrid design spaces that satisfy the persistence requirement and are near the minimum aggregate capacity points are shown in Figures 9 and 10. The battery maximum capacity for systems near the optimal points for both hybrid optimizations are in the range of 9 to 30 kWh. Points with larger battery maximum capacities were tested, but resulted in larger aggregate capacity. Points with smaller battery maximum capacities resulted in insufficient persistence values. The total generation capacity near the optimal points are similar for the two hybrid

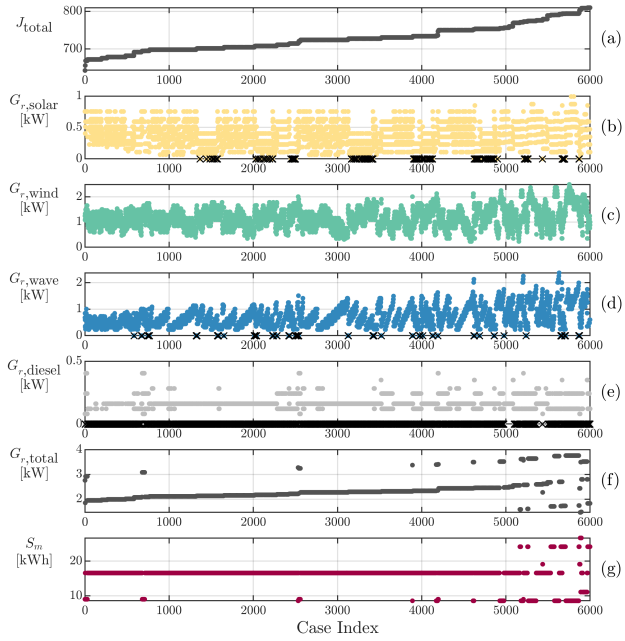

Fig. 9. Representation of the **hybrid design space excluding the current turbine**. Each case index (x-axis) corresponds to a unique point in the design space. Each point is defined by the value of each free parameter: generator rated capacities (b-e) and battery maximum capacity (g). Black x-markers correspond to a zero - capacity generator for that resource and case index. The sum of generator rated capacities is the total generation capacity at each index (f). To show how the power system definition changes across the space, the grid points where the power system satisfied the persistence requirement ($a_{\text{sim}} > 99\%$) are sorted by increasing aggregate capacity (a). While the algorithm tested over 10^4 points for this optimization, only the first 6000 points are shown to resolve behavior near the minimum aggregate capacity point (case index 1).

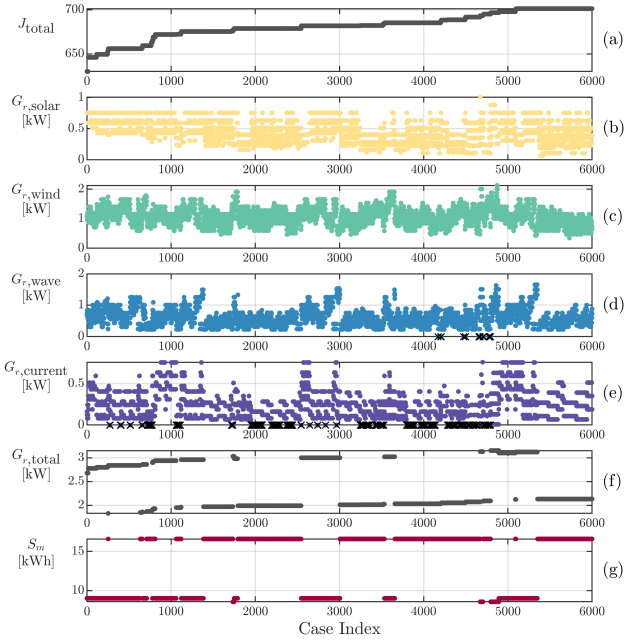

Fig. 10. Representation of the **hybrid design space excluding the diesel generator** as for Figure 9.

optimization spaces (2 to 4 kW) (Figures 9f and 10f). The range of individual generator capacities in the systems shows how the distribution of the total generation can vary, yet satisfy the persistence requirement. In addition, combinations with similar objective function cost do not always include all possible generation sources.

IV. Discussion

The hybrid optimization results presented were generated using the "persistence with multi-telescoping" algorithm. Similar optimizations were attempted using solely the telescoping refinement or persistence band algorithms. The telescoping refinement is prone to "zooming-in" on local minimums based on the lowest aggregate capacity points resolved in the coarsest design space. If the minimum in a coarse space is not close to the global minimum, then the telescoping refinement algorithm will never search near the global minimum. The persistence band algorithm is less likely to find local minimums, but the number of points tested by this algorithm is orders of magnitude larger than the number tested by telescoping, which increases runtime per iteration. Additionally, because the grid discretization is only doubled in each iteration, more iterations are required to reach a sufficiently fine grid discretization. Because of this, the run time for a persistence-only algorithm is infeasible, even with high-performance computing resources. Because of this the "persistence with multi-telescoping" algorithm was developed to use the benefits of each algorithm, while potentially avoiding their limitations. The persistence algorithm run-time is only infeasible for iterations ≥ 4 (when the iteration time becomes infeasible is specific to the optimization space). Therefore, only running the persistence algorithm three times is computationally feasible. Following this, the telescoping algorithm quickly refines the space around multiple candidate cases for lowest aggregate capacity. As described in Section II-D, this algorithm's behavior is subject to the input parameters (number of points in each telescoping grid, definition of the persistence band, and definition of the points of interest for the telescoping iterations). Multiple versions of this algorithm were tested with varying definitions of these input parameters, and the final values were based on a balance of computational speed with result consistency and accuracy. For this optimization problem, the results are particularly sensitive to the definition of the persistence band, and narrowing the band definition can cause the algorithm to solve to a significantly larger "minimum" aggregate capacity. Sensitivity studies with varying input values are required for validation of results.

V. Conclusions and Future Work

Despite the optimization difficulty, the results from this preliminary analysis show that the renewable resources are well matched and there is a benefit to hybridization for an ocean observation system in Argentine Basin. The results also show that a purely

renewable energy system can satisfy the instrumentation and UUV recharge load with a smaller aggregate capacity than the hybrid system with a diesel generator. However, the definition of an "optimal" system is dependent on the optimization target. Minimum aggregate capacity used in this analysis does not take into account that each generator's unit mass is different, or differences in the unit economic cost of each power system component. Future work will focus on expanding the model to optimize for lowest system economic cost. This requires parametric models for the platform and mooring as prior work has shown that these costs are significant [18]. Based on our experience with this preliminary analysis, we expect that changing the optimization target will increase the design space complexity and increase the difficulty of identifying global minimum values. Therefore, economic optimization targets may require more sophisticated algorithms.

Data Availability

The hybrid optimization code is available at https://github.com/smp52-uw/OO-Hybrid.

Acknowledgement

The authors gratefully acknowledge discussions with Josh Hamel about potential algorithms to explore the design space. In addition, thanks to Kristin Zeiden for providing code to download the current velocity data from HYCOM, and Morteza Derakhti for providing guidance and access to UW's high-performance computing resources.

References

[1] P. Miloslavich *et al.*, "Essential ocean variables for global sustained observations of biodiversity and ecosystem changes," *Global Change Biology*, vol. 24, no. 6, pp. 2416–2433, 2018.

[2] R. Green, A. Copping, R. Cavagnaro, D. Rose, D. Overhus, and D. Jenne, "Enabling power at sea: Opportunities for expanded ocean observations through marine renewable energy integration," *Oceans 2019 MTS/IEEE Seattle*, 2019.

[3] J. H. Greer and C. S. Niederman, "Power for data buoys and other remote stations." in *OCEAN 75 Conference*. IEEE (75 CHO 995-1 OEC), 1975, pp. 736–740.

[4] P. C. Kohler, L. LeBlanc, and J. Elliott, "Scoop-ndbc's new ocean observing system," in *OCEANS 2015-MTS/IEEE Washington*. IEEE, 2015, pp. 1–5.

[5] N. R. Pettigrew, C. S. Roesler, F. Neville, and H. E. Deese, "An operational real-time ocean sensor network in the gulf of maine," in *GeoSensor Networks: Second International Conference, GSN 2006, Boston, MA, USA, October 1-3, 2006, Revised Selected and Invited Papers*. Springer, 2008, pp. 213–238.

[6] A. Hamilton, F. Cazenave, D. Forbush, R. G. Coe, and G. Bacelli, "The mbari-wec: a power source for ocean sensing," *Journal of Ocean Engineering and Marine Energy*, vol. 7, pp. 189–200, 5 2021.

[7] J. Joslin *et al.*, "The wave-powered adaptable monitoring package: hardware design, installation, and deployment," in *Proceedings of the 13th European Wave and Tidal Energy Conference, Naples, Italy*, 2019, pp. 1–6.

[8] C. Dizon, R. J. Cavagnaro, B. Robertson, and T. K. Brekken, "Modular horizontal pendulum wave energy converter: Exploring feasibility to power ocean observation applications in the us pacific northwest," *IET Renewable Power Generation*, vol. 15, no. 14, pp. 3354–3367, 2021.

[9] C. L. Oikonomou, R. P. Gomes, and L. M. Gato, "Unveiling the potential of using a spar-buoy oscillating-water-column wave energy converter for low-power stand-alone applications," *Applied Energy*, vol. 292, 6 2021.

[10] R. Carolan, B. Walsh, M. Boland, T. Dooley, and T. Kelly, "The design and construction of a prototype wasp-a novel wave measuring buoy," in *Proceedings of 13th European wave and tidal energy conference, Napoli, Italy*, 2019, pp. 1594–1.

[11] B. Kesavakumar, M. ArulMuthiah, S. Elango, D. Gowthaman, P. Kaliyaperumal, P. Senthilkumar, R. Sridharan, and R. Venkatesan, "Design of optimal power source for niot offshore moored buoy system," in *2013 Ocean Electronics (SYMPOL)*. IEEE, 2013, pp. 189–195.

[12] J. M. Ayers and K. Richter, "The potential of small-scale turbines and microbial fuel cells to support persistent oceanographic sensors," in *OCEANS 2016 MTS/IEEE Monterey*. IEEE, 2016, pp. 1–6.

[13] G. Chew, D. G. Pelaccio, and D. Johnson, "Study of power system upgrades for ndbc buoys," in *OCEANS'02 MTS/IEEE*, vol. 1. IEEE, 2002, pp. 388–395.

[14] I. McLeod and J. V. Ringwood, "Powering data buoys using wave energy: a review of possibilities," *Journal of Ocean Engineering and Marine Energy*, 6 2022.

[15] D. A. Gemme, H. R. Greene, T. A. Tucker, R. B. Sepe, and S. P. Bastien, "Hybrid resonant wave energy harvesting buoy for sensor applications," in *2013 OCEANS-San Diego*. IEEE, 2013, pp. 1–6.

[16] A. Hegarty, D. Toal, E. Omerdic, and G. Westbrook, "Broadening out the working footprint of a cabled seabed observatory using an interconnected surface buoy, and examining the potential to achieve similar utility from a stand-alone buoyed platform," Ph.D. dissertation, Ph. D. thesis, Centre for Robotics and Intelligent Systems, University of Limerick, 2021.

[17] T. Lambert, P. Gilman, and P. Lilienthal, "Micropower system modeling with homer," *Integration of alternative sources of energy*, vol. 1, no. 1, pp. 379–385, 2006.

[18] T. Dillon, "Economic, system, and community-based optimization of off-grid wave energy conversion," Ph.D. dissertation, University of Washington, 2023.

[19] T. Dillon, B. Maurer, M. Lawson, D. S. Jenne, D. Manalang, E. Baca, and B. Polagye, "Cost-optimal wave-powered persistent oceanographic observation," *Renewable Energy*, vol. 181, pp. 504–521, 2022.

[20] C. Jamroen, N. Yonsiri, T. Odthon, N. Wisitthiwong, and S. Janreung, "A standalone photovoltaic/battery energy-powered water quality monitoring system based on narrowband internet of things for aquaculture: Design and implementation," *Smart Agricultural Technology*, vol. 3, p. 100072, 2 2023.

[21] B. Xu, A. Oudalov, A. Ulbig, G. Andersson, and D. S. Kirschen, "Modeling of lithium-ion battery degradation for cell life assessment," *IEEE Transactions on Smart Grid*, vol. 9, pp. 1131–1140, 2018.

[22] B. Polagye, J. Joslin, P. Murphy, E. Cotter, M. Scott, P. Gibbs, C. Bassett, and A. Stewart, "Adaptable monitoring package development and deployment: Lessons learned for integrated instrumentation at marine energy sites," *Journal of Marine Science and Engineering*, vol. 8, no. 8, p. 553, 2020.

[23] L. M. Smith, J. A. Barth, D. S. Kelley, A. Plueddemann, I. Rodero, G. A. Ulses, M. F. Vardaro, and R. Weller, "The ocean observatories initiative," *Oceanography*, vol. 31, pp. 16–35, 2018. [Online]. Available: https://www.jstor.org/stable/10.2307/26307783

[24] R. Bleck, "An oceanic general circulation model framed in hybrid isopycnic-cartesian coordinates," *Ocean modelling*, vol. 4, no. 1, pp. 55–88, 2002.

[25] D. C. Jordan and S. R. Kurtz, "Photovoltaic degradation rates—an analytical review," *Progress in photovoltaics: Research and Applications*, vol. 21, no. 1, pp. 12–29, 2013.

[26] A. Standard, "Awea small wind turbine performance and safety standard," Technical report, American Wind Energy Association, Tech. Rep., 2009.

[27] V. S. Neary, M. Previsic, R. A. Jepsen, M. J. Lawson, Y.-H. Yu, A. E. Copping, A. A. Fontaine, K. C. Hallett, and D. K. Murray, "Sandia report methodology for design and economic analysis of marine energy conversion (mec) technologies," Sandia National l Laboratories, Tech. Rep., 2014. [Online]. Available: http://www.ntis.gov/help/ordermethods.asp?loc=7-4-0#online

[28] *The New 400 watt turbine! Owner's Manual*, 1999.

[29] D. Corbus, H. Link, S. Butterfield, C. Stork, and C. Newcomb, "Certification testing for small wind turbines," National Renewable Energy Lab.(NREL), Golden, CO (United States), Tech. Rep., 1999.

[30] "Bu-205: Types of lithium-ion," https://batteryuniversity.com/article/bu-205-types-of-lithium-ion, Oct 2022, accessed: 2023-06-05.

[31] "Aluminum sheet and plate," https://www.russelmetals.com/en/company/acier-leroux/product/aluminum/aluminum-sheet-plate/, 2019, accessed: 2023-06-05.